

STAR FORMATION IN SATELLITE GALAXIES¹

C. M. GUTIÉRREZ

Instituto de Astrofísica de Canarias, c/ Via Lactea s/n, La Laguna, E-38205 Tenerife, Spain; cgc@iac.es

M. S. ALONSO²

Consejo Nacional de Investigación Científicas y Técnicas, Buenos Aires, Argentina; salonso@casleo.gov.ar

J. G. FUNES, SJ

Vatican Observatory, University of Arizona, Tucson, AZ 85721

AND

M. B. RIBEIRO

Instituto de Física, Universidade Federal do Rio de Janeiro, Rio de Janeiro, Brazil

Received 2005 December 1; accepted 2006 March 25

ABSTRACT

We present narrowband observations of the H α emission in a sample of 31 satellites orbiting isolated giant spiral galaxies. The sample studied spans the range $-19 \text{ mag} < M_B < -15 \text{ mag}$. H α emission was detected in all the spiral and irregular objects with fluxes in the range $(1.15\text{--}49.80) \times 10^{-14} \text{ ergs cm}^{-2} \text{ s}^{-1}$. The average and maximum values for the current star formation rates are 0.68 and 3.66 $M_\odot \text{ yr}^{-1}$, respectively. Maps of the spatial distribution of ionized gas are presented. The star-forming regions show a rich structure in which frequently discrete complexes are imposed over more diffuse structures. In general, the current star formation rates are smaller than the mean values in the past, obtained from the stellar content; this probably indicates a declining rate with time in the generation of new stars. However, the reserve of gas is enough to continue fueling the current levels of star formation activity for at least another Hubble time. Four of the objects (NGC 2718b, NGC 4541e, and NGC 5965a₁ and NGC 5965a₂) with higher current star formation rates show clear signs of interaction with close companions of comparable brightness at projected distances of 25, 20, and 2 kpc, respectively. The only two galaxies in our sample that do not show star formation activity are members of these interacting systems, and it is unclear if this is a consequence of intrinsic properties (both are early Hubble types) or if it is related to possible disruption of the external parts due to the interaction. In the case of the pair NGC 2718a-2718b there are indications of gas transport between the galaxies.

Key words: galaxies: evolution — galaxies: fundamental parameters — galaxies: photometry — galaxies: structure

1. INTRODUCTION

Cold dark matter (CDM) cosmologies predict a hierarchical scenario (e.g., White & Rees 1978) in which small structures are formed first, and then by several processes of merging, accretion, etc., larger structures are generated. Currently, one of the most discussed questions in this field is the so-called missing satellite problem; in fact, semianalytic models (Kauffmann et al. 1993) and numerical simulations (Klypin et al. 1999; Moore et al. 1999) of small structure formation in CDM cosmologies predict a number of satellites in the halos of large galaxies an order of magnitude larger than the observed counts in the Local Group. A possible observational incompleteness of a factor up to 3 of the known population of dwarfs orbiting the Milky Way, as has been evaluated by Willman et al. (2004), is not enough to solve the discrepancy. It has also been proposed that star formation in low-mass structures could be inhibited by a strong photoionizing background (Somerville 2002), especially at low redshift (Dijkstra et al. 2004).

Reconstructing the evolutionary history of satellites in galactic halos is, then, essential for validating the main predictions

of these models. This requires study of the role of physical processes such as interactions, mass losses, morphological transformations, and star formation. Obviously, the best studied are the Milky Way and Andromeda halos, although extending the study to other host galaxies is necessary for studying possible variations from halo to halo, which probably depends on the host mass, the merging history, and the environment. That was our motivation to start an observational program that comprises photometry in optical broadband and narrowband filters for a sample of satellites orbiting external giant spiral galaxies. In previous articles (Gutiérrez et al. 2002; Gutiérrez & Azzaro 2004) we have analyzed the morphology and photometry of about 60 such objects. This analysis enabled us to validate and extend the relations found in the satellites of the Local Group. In this paper we use narrowband observations in H α to estimate the current star formation rate (SFR) of a subsample comprising most of the late-type objects. We analyze the evolution of star-forming activity with time and the relation to morphological type, H I mass, and environment. The paper is organized as follows. Section 2 presents the observations and data reduction; § 3 and the Appendix present the images and analyze qualitatively the H α maps of each object; the SFR estimates are presented in § 4; the relation between interactions and star formation and the cosmological evolution of star formation activity are discussed in §§ 5 and 6; and finally, § 7 presents the conclusions.

¹ Based on observations with the Vatican Advanced Technology Telescope: the Alice P. Lennon Telescope and the Thomas J. Bannan Astrophysics Facility.

² Marie Curie Fellow; Instituto de Astrofísica de Canarias, c/ Via Lactea s/n, La Laguna, E-38205 Tenerife, Spain.

2. OBSERVING PROGRAM

2.1. *The Sample*

The initial sample is the catalog of satellite galaxies compiled by Zaritsky et al. (1997). The catalog contains 115 objects orbiting 69 primary isolated spiral galaxies. Basically, the satellites were selected according to their relative brightness (at least 2.2 mag fainter than their parents), projected distances (< 500 kpc), and relative velocity (< 500 km s $^{-1}$) from the primaries. The objects analyzed here correspond to a subsample comprising most of the objects classified by Gutiérrez & Azzaro (2004) as spiral or irregular galaxies. In total, 31 objects have been observed and analyzed (most of the late-type objects observable from the northern hemisphere). The objects span a large range in luminosity ($-19 < M_B < -15$) and constitute a sample useful for statistical studies of the population of late-type galaxies present in the halos of large spiral galaxies.

2.2. *Observations and Data Reduction*

The H α and broadband images for continuum estimation were acquired during three observing runs of seven nights each in 2001 December, 2002 May, and 2002 December with the 1.8 m Vatican Advanced Technology Telescope at the Mount Graham International Observatory. Most of the observations analyzed here were obtained in the first two runs and in photometric conditions (for only two of the galaxies was it possible to make an absolute direct calibration; see § 3). A back-illuminated 2048 \times 2048 Loral CCD was used as the detector at the aplanatic Gregorian focus, $f/9$. It yielded a field of view of $6'.4 \times 6'.4$ with an image scale of $0''.4$ pixel $^{-1}$ after 2×2 pixel binning. The seeing varied between $1''.1$ and $2''.3$ with a mean value of $1''.5$. For each galaxy we have obtained typically 3×1800 s narrowband images using appropriate interference filters with ~ 70 Å widths that isolate the spectral region characterized by the redshifted H α and [N II] $\lambda\lambda 6548, 6583$ emission lines. To cover the range in velocity spanned by the galaxies presented in this work, three filters were needed with central wavelengths of 6584.7, 6632.8, and 6736.2 Å (another existing filter centered at 6683.1 Å was not necessary for any of the galaxies analyzed in this work). The nominal normalized spectral responses of these filters are presented in Figure 1. Table 1 presents a summary of the observations and properties of the images obtained. Each filter is denoted according to its central wavelength in nanometers.

For absolute astronomical calibration we observed spectrophotometric standard stars from the list provided by Oke (1990). In general, we observed one of these stars just before or after the narrowband observations for each galaxy. In each case stars were selected for similar air mass rather than to calibrate the target. The exposure times for these stars range between 12 and 300 s, depending obviously on the magnitude of the star. These details are shown in Table 1. The data were reduced using IRAF packages.³ We performed standard data reduction, comprising bias subtraction, flat-field correction using sky twilight observations in the appropriate filters, alignment of R and narrowband images, and co-addition of the narrowband images. This combination eliminates most of the artifacts due to bad pixels or cosmic rays.

To isolate the possible H α emission of the targeted galaxies, the contribution of the stellar continuum emission of the galaxy needs to be removed. This was done by appropriately scaling the

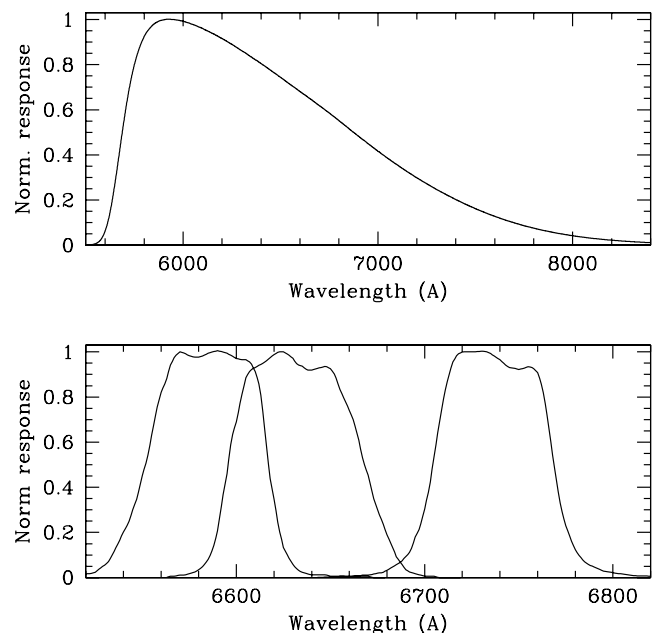


FIG. 1.—Normalized response of the R broadband filter (*top*) and the three narrowband filters (*bottom*) used during the observations presented in this paper.

R -band image and subtracting it from the H α images. The scaling factor was estimated by comparing the brightness of several field stars in the broad and narrow bands, respectively. We measured the flux of these stars in a circular aperture ~ 6 FWHMs of the image. Depending on the field, the number of stars considered was in the range 3–12, with a typical number of 5.

3. IMAGES OF THE SATELLITE GALAXIES

The R -band and H α images, after continuum subtraction, are presented in Figures 2, 3, and 4. We have detected H α emission in all but two galaxies. For most of the galaxies, the H α emission shows a complex morphology in which it is possible to discern diffuse and discrete structures. A description of these images is presented in the Appendix. The identification of interacting systems is based on spatial proximity and on the presence of features in the R band, such as a bridge in the case of the pair NGC 2718a-2718b, tidal streams in the pair NGC 4541b-4541e, and distortion of the outer isophotes in the case of the two components of NGC 5965a. For the other galaxies there is also some evidence of current or past interactions on the basis of the proximity to the parent (NGC 3154a), possible companions with unknown redshift (NGC 3735a, NGC 4030b, NGC 4541a, and NGC 6181a), knots differentiated from the main body of the galaxy having strong star formation activity (NGC 1961b, NGC 5899a, and NGC 7678a), or the presence of possible tidal galaxies (as in NGC 2775c).

4. H α LUMINOSITIES AND STAR FORMATION RATES

We use the SExtractor software (Bertin & Arnouts 1996) to carry out photometry of the galaxies in the broadband and narrowband filters. We consider two possible estimates for the total flux of the galaxies. The first is the integrated flux in a predefined aperture (the same as for the narrow and broad filter), and the second is the flux in the automatic aperture computed in SExtractor according to the extrapolation proposed by Kron (1980). In general, we note that the first method gives more robust values for those galaxies that are more irregular, while the second is

³ IRAF is the Image Reduction and Analysis Facility, written and supported by the IRAF programming group at the National Optical Astronomy Observatory in Tucson, Arizona.

TABLE 1
LOG OF THE OBSERVATIONS

Galaxy (1)	Epoch (2)	t_R (s) (3)	$t_{H\alpha}$ (s) (4)	FWHM (R) (arcsec) (5)	FWHM ($H\alpha$) (arcsec) (6)	Calibration Star (7)	$H\alpha$ Filter (8)
NGC 488c.....	2001 Dec	1200	3×1800	2.2	1.8	BD +75 325	663
NGC 772b.....	2001 Dec	1200	3×1800	1.5	1.6	BD +75 325	663
NGC 772c.....	2001 Dec	1200	3×1800	1.3	1.7	GD 50	663
NGC 1517a.....	2001 Dec	900	3×1800	1.6	1.8	BD +75 325	663
NGC 1620a.....	2001 Dec	180	3×1800	1.6	2.1	BD +75 325	663
NGC 1961a.....	2001 Dec	900	3×1800	1.6	1.6	G193-74	663
NGC 1961b.....	2001 Dec	1200	3×1800	1.7	1.4	BD +75 325	663
NGC 1961c.....	2001 Dec	1200	3×1800	1.1	1.2	BD +75 325	663
NGC 2424b.....	2001 Dec	1200	3×1800	1.6	1.6	...	663
NGC 2718a.....	2002 May	900	3×1800	1.5	1.1	Feige 34	663
NGC 2718b.....	2002 May	900	3×1800	1.5	1.1	Feige 34	663
NGC 2775a.....	2001 Dec	300	3×1800	1.2	1.5	BD +75 325	658
NGC 2775c.....	2001 Dec	1200	3×1800	1.3	1.4	BD +75 325	658
NGC 2916a.....	2001 Dec	1200	3×1800	1.7	1.5	BD +75 325	663
NGC 3043a.....	2001 Dec	1200	3×1800	1.6	1.2	BD +75 325	663
NGC 3154a.....	2001 Dec	1200	3×1800	1.1	1.1	BD +75 325	673
NGC 3735a.....	2001 Dec	1200	3×1800	1.2	1.4	BD +75 325	663
NGC 4030b.....	2002 May	1200	3×1800	1.4	1.7	Feige 66	658
NGC 4541a.....	2002 May	1200	3×1800	1.6	1.6	Feige 34	673
NGC 4541b.....	2002 May	1200	3×1800	1.6	1.6	Feige 34	673
NGC 4541e.....	2002 May	1200	3×1800	1.6	1.6	Feige 34	673
NGC 4725a.....	2002 May	1200	3×1800	1.2	1.3	BD +33 2642	658
NGC 5248a.....	2002 May	1200	3×1800	1.1	1.2	BD +33 2642	658
NGC 5248b.....	2002 May	600	3×1800	1.8	1.7	Hz 44	658
NGC 5899a.....	2002 May	1800	3×1800	1.4	1.4	BD +33 2642	663
NGC 5962d.....	2002 May	1200	3×1800	1.1	1.3	BD +33 2642	663
NGC 5965a ₁	2002 May	600	3×1800	1.4	1.2	BD +33 2642	663
NGC 5965a ₂	2002 May	600	3×1800	1.4	1.2	BD +33 2642	663
NGC 6181a.....	2002 May	600	3×1800	1.2	1.2	BD +33 2642	663
NGC 7137a.....	2002 Dec	500	3×1200	2.2	2.3	...	658
NGC 7678a.....	2001 Dec	1200	3×1800	1.4	1.6	BD +75 325	663

more appropriate for objects with a well-defined regular profile. In the cases in which a fixed aperture was chosen, we checked that the estimated fluxes were similar to those computed with the subroutine PHOT of IRAF. For the absolute calibration and estimation of $H\alpha$ emission, we followed the procedure detailed in Gil de Paz et al. (2003). Because of the width of our narrow filters, the emission also includes the contribution of $[N II]$, for which an accurate subtraction would require spectroscopic observations.

One of the objects (NGC 4030b) was observed at two epochs (2001 December and 2002 May). We think that the $\sim 10\%$ difference between the estimates of $H\alpha$ fluxes in both observations (1.33 and 1.46×10^{-14} ergs $\text{cm}^{-2} \text{s}^{-1}$ for the observations of December and May, respectively) is representative of the statistical uncertainty of our procedure. Another test was to observe the apparently noninteracting early-type galaxy NGC 1620b, for which we do not in principle expect significant levels of star-forming activity. For this galaxy we estimate an $H\alpha$ flux after continuum subtraction of -0.87×10^{-14} ergs $\text{cm}^{-2} \text{s}^{-1}$, which in absolute value is well below any of the detections of $H\alpha$ emission. We think that this negative value is not entirely due to the uncertainties in the estimate but indicates $H\alpha$ in absorption, as is commonly found in early-type galaxies (Kennicutt 1992).

The $H\alpha$ equivalent widths (EWs) represent the ratio between the $H\alpha$ emission and the continuum averaged over the full galaxy. Figure 4 shows the relation between the relative flux of the $H\alpha$ emission and the morphological type. The mean values and

1σ dispersions in $H\alpha$ EWs are 16.4 ± 5.1 , 24.3 ± 9.6 , and 18.9 ± 7.7 for types 2 (Irr), 3 (Sb/Sc), and 4 (Sa), respectively. The mean values found for the different morphological types of noninteracting objects are similar, and therefore we do not notice differences in $H\alpha$ EWs with morphological types as found by other authors (e.g., Kennicutt 1998). The much higher $H\alpha$ EW values found for four of the satellites in interaction indicate that their activity is directly related to current interaction processes.

The $H\alpha$ EWs were converted into fluxes ($f_{H\alpha}$) following the calibration explained in § 2; $f_{H\alpha}$ was then converted into absolute luminosity according to $L_{H\alpha} = 4\pi D^2 f_{H\alpha}$. To estimate distances, we took the recessional velocity of the respective parent galaxy (the satellite is more affected by the peculiar velocities). In any case, the difference in the estimated luminosity would be relevant only for a few systems at very low redshift and with comparatively large differences in velocity between the parent and the satellite (NGC 4030b is the extreme case). For the Hubble constant we assumed $H_0 = 72$ km s^{-1} Mpc $^{-1}$. The $H\alpha$ fluxes and luminosities are presented in Table 2. For the galaxies with $H\alpha$ emission, the luminosities are in the range $\log L_{H\alpha} = 38.85$ – 41.66 ergs s^{-1} . A histogram with the distribution of $H\alpha$ luminosities is presented in Figure 5.

To convert $L_{H\alpha}$ to current SFRs, we use the calibration provided by Kennicutt (1998), $\text{SFR} (M_\odot \text{ yr}^{-1}) = 7.9 \times 10^{-42} L_{H\alpha}$ ergs s^{-1} , which assumes a Salpeter (Salpeter 1955) initial mass function between 10^{-1} and $10^2 M_\odot$. Because we do not have observations of other Balmer lines (specifically $H\beta$), we did not

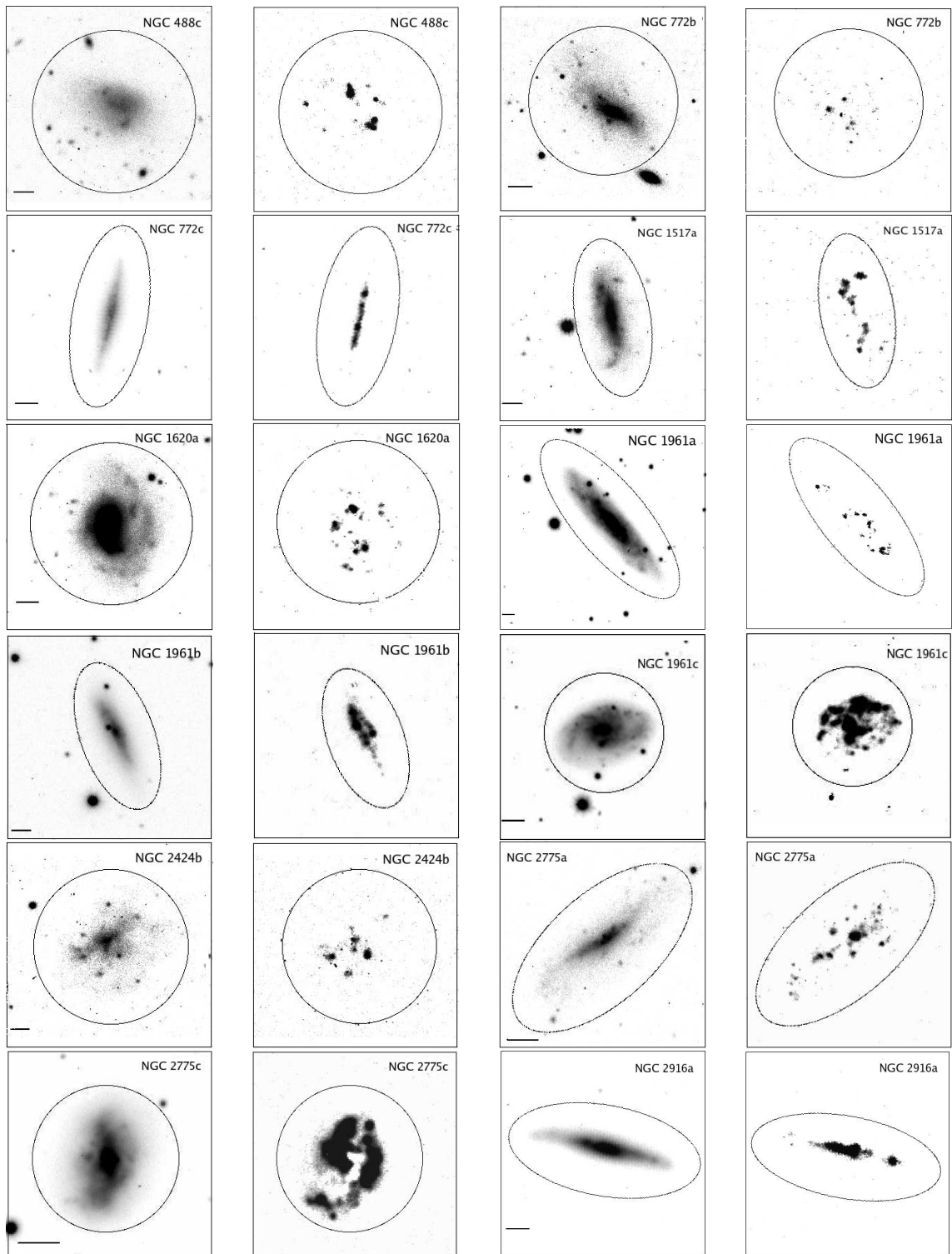


FIG. 2.—Images of the sample of objects analyzed in this work. For each object are presented the R -band and $H\alpha$ images after continuum subtraction. North is up, and east is to the left. The small line at the bottom is scaled to an angular size of $10''$.

apply any correction for internal extinction. The values obtained for the current SFR are presented in Table 3, column (2). Figure 6 shows SFR as a function of luminosity in the B band. A significant correlation (although with a large scatter) exists. A similar tendency was found in the sample of blue compact galaxies studied by Kong (2004), and with the much larger sample of $\approx 10^5$ Sloan Digital Sky Survey galaxies studied by Brinchmann et al. (2004). Four of the interacting satellite galaxies (indicated

by filled circles in the figure) show a similar tendency, although they clearly have higher levels of star formation than noninteracting galaxies with similar luminosities.

4.1. Comparison with Previous Star Formation Rate Estimations

The SFRs of some of the objects analyzed in this work have been previously estimated by other authors. In some cases, their

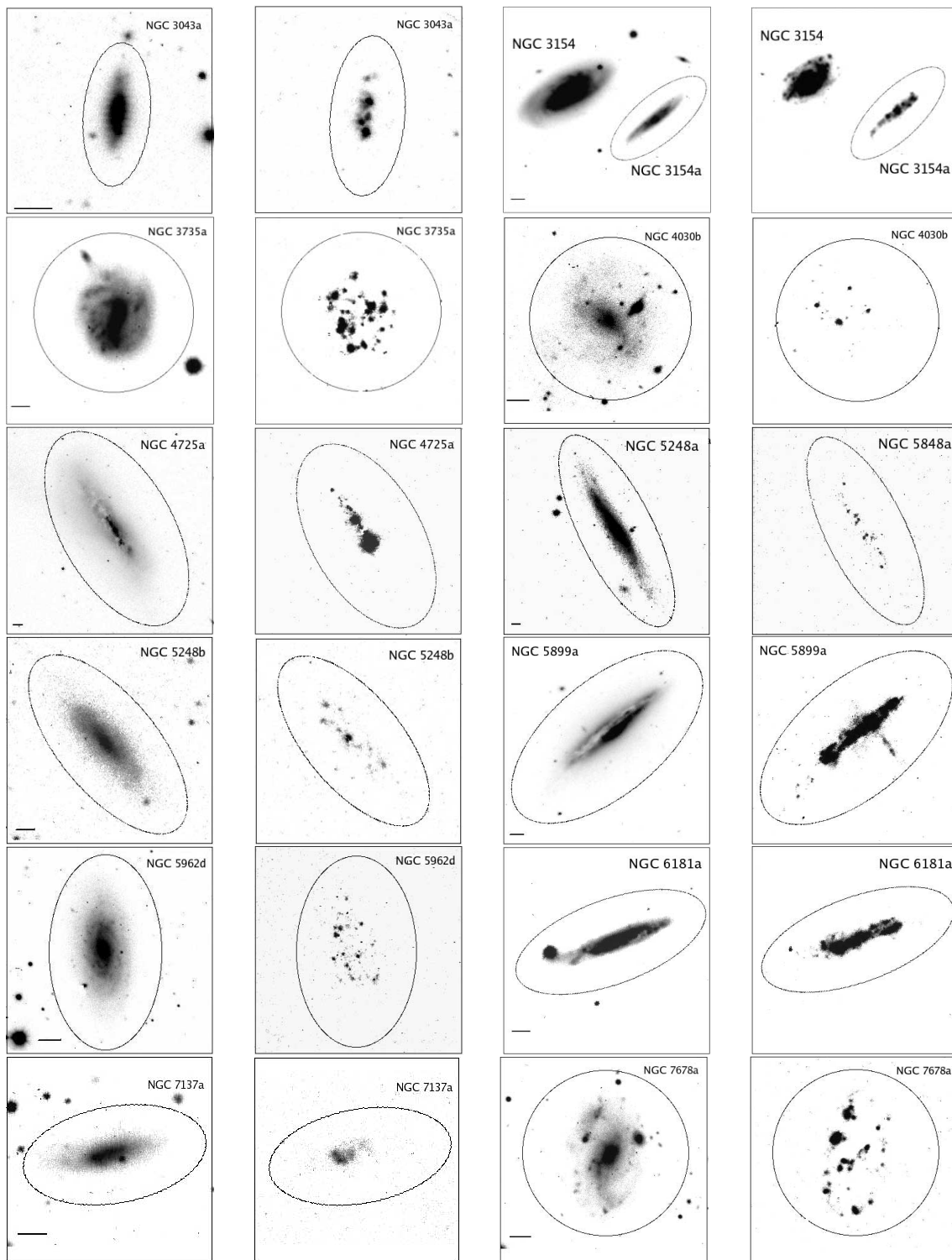


FIG. 2.—Continued

SFRs have been estimated from $H\alpha$ measurements in narrow-band images or spectroscopy, while in others, SFRs have been obtained from observations in the far-IR or radio. Below we compare our results with these previous studies compiled from the literature.

NGC 2718a and NGC 2718b: Mendez et al. (1999) have estimated a luminosity of $40.87 \text{ ergs s}^{-1}$ for the component NGC 2718b, which is in good agreement with our value of $40.91 \text{ ergs s}^{-1}$. However, they derived an EW of 260 \AA for the $H\alpha$ emission

of this galaxy, which is a factor >2 larger than our value. Our estimate of $H\alpha$ EW for this galaxy is also a factor of ~ 2.5 smaller than that presented by Kong et al. (2002) from long-slit observations. However, our EW and $H\alpha$ luminosities are in very good agreement with the estimates by Gil de Paz et al. (2003), 120 \AA and $40.85 \text{ ergs s}^{-1}$, respectively. So, considering only the three measurements based on narrowband imaging, it seems that the three estimates of the $H\alpha$ luminosities are in agreement, but they are in clear disagreement with EWs derived from long-slit

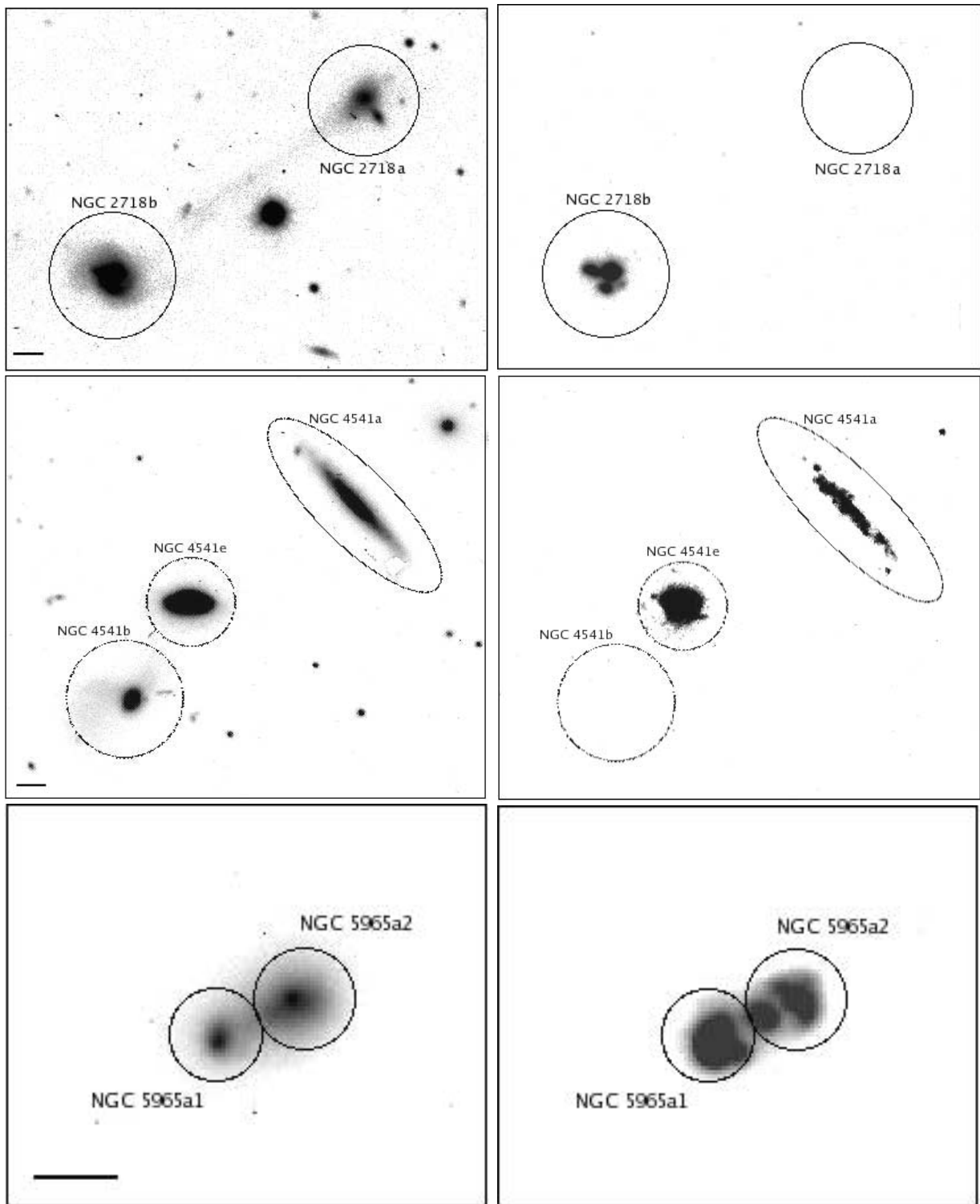


FIG. 3.—Same as Fig. 2, but for the three sets of interacting satellite galaxies: NGC 2718a-2718b, NGC 4541a and NGC 4541b-4541e, and NGC 5965a₁-5965a₂.

spectra. Although the reason for this discrepancy between the estimates obtained with each technique is unclear, it could be related to the irregular spatial distribution of the H α features. This renders inaccurate the extrapolation of the H α intensity from the area covered by the long slit of the whole galaxy.

NGC 5965a₁ and 5965a₂: The estimates carried out previously by other authors enclose the H α flux for the whole system. For this, our estimate of the H α flux is 27.2×10^{-14} ergs s $^{-1}$ cm $^{-2}$, which is in good agreement with the value of $30 \pm 3 \times 10^{-14}$ ergs

s $^{-1}$ cm $^{-2}$ measured by Gil de Paz et al. (2003). For this pair, Bell (2003) obtained an SFR of $0.8 M_{\odot} \text{ yr}^{-1}$ from radio measurement, while Hopkins et al. (2002) obtained 0.8 and $1.7 M_{\odot} \text{ yr}^{-1}$ from observations at $60 \mu\text{m}$ and 1.4 GHz, respectively. However, these authors use a different distance to the galaxy (53.2 Mpc) instead of the value 47.6 Mpc that we have used. Converting our results to their distance scale, we would obtain SFR = $0.72 M_{\odot} \text{ yr}^{-1}$, which is within 25% of the value derived by these authors from the luminosity at $60 \mu\text{m}$. Given the different uncertainties and

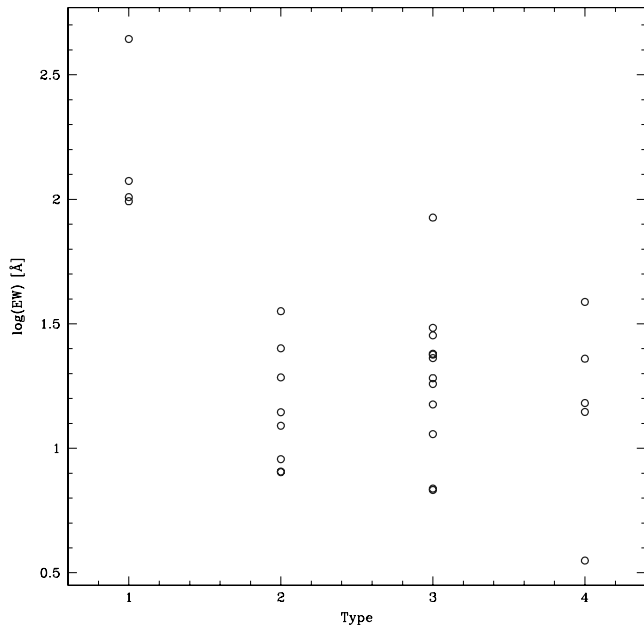


FIG. 4.—H α EWs as a function of galactic type: (1) objects in interaction, (2) irregular galaxies, (3) Sb/Sc, and (4) Sa.

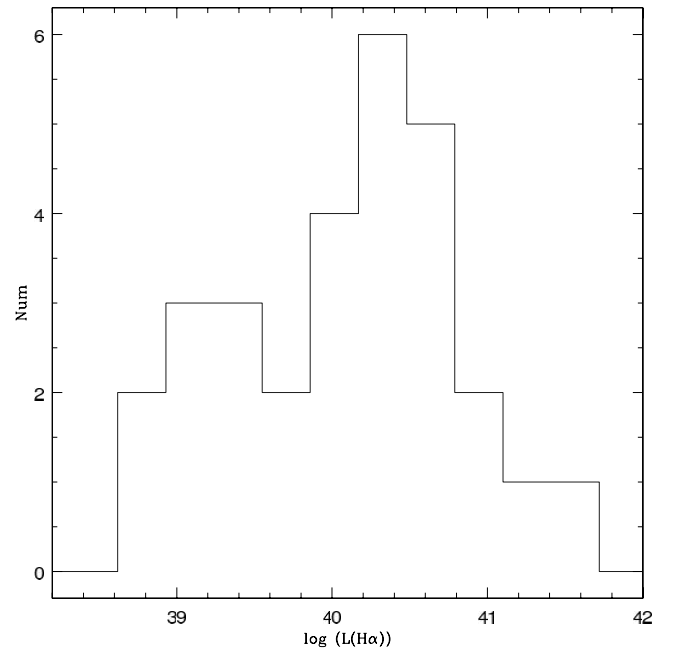


FIG. 5.—Distribution of H α luminosities for the sample of satellite galaxies analyzed in this paper.

TABLE 2
H α EQUIVALENT WIDTHS, FLUXES, AND LUMINOSITIES

Galaxy (1)	r_p (kpc) (2)	$EW_{H\alpha}$ (Å) (3)	H α Flux (10^{-14} ergs cm $^{-2}$ s $^{-1}$) (4)	$\log L(H\alpha)$ (ergs s $^{-1}$) (5)
NGC 488c.....	116	8.07	1.15	39.13
NGC 772b.....	390	13.97	2.15	39.48
NGC 772c.....	429	15.19	4.63	39.81
NGC 1517a.....	130	23.76	9.33	40.41
NGC 1620a.....	227	8.03	2.75	39.89
NGC 1961a.....	214	6.89	7.97	40.45
NGC 1961b.....	139	15.01	9.90	40.55
NGC 1961c.....	120	28.42	29.00	41.01
NGC 2424b.....	182	35.52
NGC 2718a.....	102	-11.64
NGC 2718b.....	82	118.58	23.80	40.91
NGC 2775a.....	401	23.99	9.53	39.61
NGC 2775c.....	64	19.26	21.40	39.96
NGC 2916a.....	71	14.01	2.66	39.93
NGC 3043a.....	263	38.72	4.02	39.92
NGC 3154a.....	19	84.40	13.00	41.11
NGC 3735a.....	192	3.54	2.01	39.53
NGC 4030b.....	414	23.03	1.46	38.85
NGC 4541a.....	193	22.89	5.48	40.78
NGC 4541b.....	228	-1.29
NGC 4541c.....	217	101.22	42.10	41.66
NGC 4725a.....	132	11.41	49.80	40.22
NGC 5248a.....	150	9.05	3.78	39.06
NGC 5248b.....	164	12.33	2.76	38.93
NGC 5899a.....	106	19.14	40.80	40.79
NGC 5962d.....	89	6.80	3.58	39.50
NGC 5965a ₁	532	440.68	16.50	40.64
NGC 5965a ₂	532	102.03	9.41	40.40
NGC 6181a.....	257	30.49	46.40	40.78
NGC 7137a.....	64	25.21	2.24	39.17
NGC 7678a.....	165	18.15	9.36	40.42

NOTE.—Observations for NGC 2424a were not taken in photometric conditions.

TABLE 3
H I MASSES, STAR FORMATION PROPERTIES, AND TIMESCALES

Galaxy (1)	SFR (M_{\odot} yr $^{-1}$) (2)	$\langle SFR \rangle_{\text{past}}$ (M_{\odot} yr $^{-1}$) (3)	$\log M_{H I}$ (M_{\odot}) (4)	t_{gas} (Gyr) (5)	t_{form} (Gyr) (6)
NGC 488c.....	0.011	0.048	8.75	51.9	12.9
NGC 772b.....	0.024	0.044	8.78	25.1	5.8
NGC 772c.....	0.051	0.107	8.80	12.4	5.1
NGC 1517a.....	0.206	0.290	9.57	17.9	2.7
NGC 1620a.....	0.062	0.149	9.35	35.5	10.7
NGC 1961a.....	0.225	0.867	9.73	23.5	12.9
NGC 1961b.....	0.279	0.447	5.5
NGC 1961c.....	0.817	0.938	3.6
NGC 2424b.....	...	0.048	9.05
NGC 2718a.....	...	0.221
NGC 2718b.....	0.640	0.081	9.50	4.8	1.8
NGC 2775a.....	0.032	0.050	9.06	37.6	13.1
NGC 2775c.....	0.072	0.123	8.74	7.8	8.4
NGC 2916a.....	0.067	0.285	9.34	32.5	17.2
NGC 3043a.....	0.066	0.073
NGC 3154a.....	1.016	0.347	1.5
NGC 3735a.....	0.027	0.222	36.1
NGC 4030b.....	0.006	0.132	8.74	95.0	128.7
NGC 4541a.....	0.476	0.486	7.3
NGC 4541b.....	...	0.382
NGC 4541c.....	3.659	1.043	1.0
NGC 4725a.....	0.132	0.336	9.21	12.0	12.6
NGC 5248a.....	0.009	0.041	8.82	70.6	19.9
NGC 5248b.....	0.007	0.057	8.45	41.7	27.3
NGC 5899a.....	0.489	0.434	9.56	7.3	4.5
NGC 5962d.....	0.025	0.230	8.56	14.4	35.1
NGC 5965a ₁	0.350	0.132	1.7
NGC 5965a ₂	0.200	0.058	1.3
NGC 6181a.....	0.476	0.421	9.36	4.8	3.8
NGC 7137a.....	0.012	0.024	8.80	54.0	7.5
NGC 7678a.....	0.208	0.400	9.39	11.5	6.7

NOTE.—H I data were collected from the LEDA catalog.

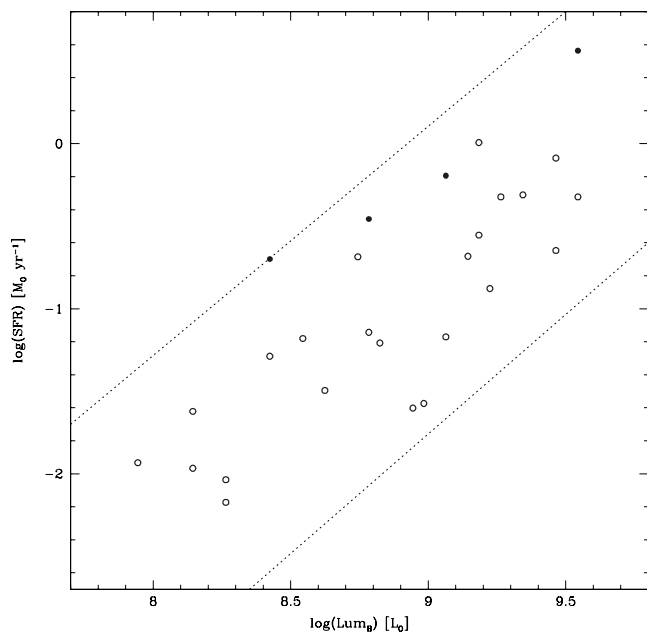


FIG. 6.—Current SFR estimated from the $H\alpha$ luminosities, as a function of luminosity in the B band. Objects in interaction have been indicated by filled circles.

assumptions in each of the methods, we consider both estimates to be in very good agreement.

5. INTERACTIONS AND STAR FORMATION

Observations and simulations have shown that galaxy interactions and mergers are powerful mechanisms for triggering star formation (e.g., Kennicutt 1998; Donzelli & Pastoriza 1997; Barton et al. 2000; see, however, Bergvall et al. 2003). Lambas et al. (2003) and Alonso et al. (2004) have carried out statistical analyses of star formation in the sample of galaxies of the Two Degree Field survey (Colless et al. 2001), finding that objects with close neighbors tend to have a higher star formation activity than those that are isolated. This tendency is more efficient for pairs situated in low-density regions. According to the studies by Sekiguchi & Wolstencroft (1992) and Donzelli & Pastoriza (1997), enhancement of the star formation activity is more likely to take place in both galaxies of the pair but tends to be higher in the fainter component. However, the analysis by Lambas et al. (2003) indicates that a large number of interacting galaxies do not show enhanced star formation activity.

Two basic types of interactions can be differentiated in the halos of giant galaxies; those between parents and satellites, and those between satellites. Both in principle can produce morphological changes and mass losses and affect the star formation activity in the interacting objects; for instance, Knebe et al. (2006), by using N -body simulations, have estimated that interactions between satellites can account for $\sim 30\%$ of the total mass loss throughout their hectic existence.

Gutiérrez et al. (2002) pointed out two clear cases of interaction (NGC 2718a-2718b and NGC 4541b-4541e) between pairs of satellites. An additional pair (the two components of NGC 5965a) was also considered by Gutiérrez & Azzaro (2004). A relatively high fraction of other satellites in our sample show morphological signs that could be attributed to present or recent interaction (see § 3 and the Appendix), but the possible companions have not been accurately identified. Our results confirm that interactions between satellites significantly affect the star formation activity.

According to Gutiérrez & Azzaro (2004) the differences in magnitudes between the two members of the pairs NGC 2718a-2718b, NGC 4541b-4541e, and NGC 5965a₁-5965a₂ are $\delta m \sim 1$ mag in the R band. In the first two cases, a high level of $H\alpha$ emission is detected in just one member of the interacting system, NGC 2718b and NGC 4541e, which are the brighter components of their respective pairs. The other two galaxies in these pairs, NGC 2718a and NGC 4541b, are the only two members of the sample analyzed that do not show $H\alpha$ emission. These two galaxies are also the only objects in our sample that were classified as early types and have been included only as members of the interacting pairs. The filaments and bridges seen in the pairs NGC 2718a-2718b and NGC 4541b-4541e do not show $H\alpha$ emission either. We propose that in the case of NGC 2718a the presence of the bridge connecting this galaxy with the companion, and the comparatively large amount of gas (see § 6) in NGC 2718b, are signs of mass transfer from one galaxy to the other. This is probably inhibiting the galaxy formation in the donor and enhancing it in the accreting galaxy. The stripping suffered by NGC 2718a could also be responsible for its morphological evolution toward early-type objects. The situation is more confused for the pair NGC 4541b-4541e, where only one of the two plumes emerging from NGC 4541b seems to point toward NGC 4541e, and there are no $H\text{ I}$ measurements in the literature for any of the two galaxies of the pair.

In the pair NGC 5965a₁-5965a₂ both members show a high level of star formation, the brighter galaxy (a₁) also being the one that has experienced the more intense SFR activity. In this case the small projected spatial distance, the absence of tidal streams or bridges, and the elongation of the isophotes through the respective companion seem to indicate that these two galaxies are experiencing their first interaction, and the gas is being strongly compressed.⁴ We have also computed the $H\alpha$ emission in an aperture enclosing both galaxies and obtained $\text{SFR} = 0.576 M_{\odot} \text{ yr}^{-1}$. This is $\sim 5\%$ higher than the result obtained by just adding the $H\alpha$ emission estimated for each component. Although compatible with the uncertainties of the method, this excess could also indicate the presence of some $H\alpha$ residual emission in the intergalactic media. The fact that in each of the interacting pairs the SFR activity is more intense in the brighter component is in disagreement with the results of Donzelli & Pastoriza (1997).

Our sample does not contain clear cases of interactions between satellites and parents, so it is not possible to estimate the relevance of such interactions to star formation activity. We note, however, that NGC 3154a, which is the object in our sample that has the smallest projected distance from its progenitor (19 kpc), is one of the more active satellites forming stars. However, we do not notice special signs of morphological distortion in this satellite.

We can roughly check whether the abundance of interacting pairs found is reasonable according to the expectations of numerical simulations in CDM models. Knebe et al. (2004) have estimated that the mean number of satellites that have at least an encounter per orbit with other satellites depends on halo age and ranges from $\sim 4\%$ (for old halos) to $\sim 58\%$ (for young halos). These encounters tend to be more frequent and faster in the internal parts of halos. The three interacting pairs found in a sample of ~ 60 satellites studied by Gutiérrez & Azzaro (2004)

⁴We consider the two components of NGC 5965a to have velocities of 3357 and 3429 km s^{-1} for NGC 5965a₂ (SBS 1533+574A) and NGC 5965a₁ (SBS 1533+574B), respectively (Y. Izotov 2005, private communication). Apparently the recessional velocity quoted in the NED for the component SBS 1533+574B is wrong.

would then require very low velocity encounters, with interactions lasting approximately one-half to one-eighth of the orbital period. This seems to contradict the observed differences in radial velocities ($\sim 50\text{--}90\text{ km s}^{-1}$) and projected distances ($\leq 20\text{ kpc}$) between the members of each pair. However, larger statistical samples are needed to make a more robust assessment.

6. CURRENT VERSUS PAST STAR FORMATION RATES

The star formation history for satellites in CDM halos has been considered by Mayer et al. (2001). These authors show that high and low surface brightness galaxies react differently to interaction with the central galaxy. In low surface brightness satellites bursts of activity occur after each pericentric passage, while in high surface brightness satellites the first burst consumes most of the gas. In both cases the activity is very inhomogeneous over cosmological times. Following the method proposed by van Zee (2001) it is possible to estimate the average SFR over the Hubble time from the total mass of stars formed. The resulting values for $\langle \text{SFR} \rangle_{\text{past}}$ for the galaxies in our sample are presented in Table 3, column (3), and are in the range $\sim 0.04\text{--}1.04 M_{\odot} \text{ yr}^{-1}$. For most of the galaxies, these values are larger than the current SFRs as estimated from the $H\alpha$ luminosities. The normalized distributions of the current and past SFR are shown in Figure 7. It is worth noting that the current SFR spans a large range of values extending the distribution to very low values. The histogram of $\langle \text{SFR} \rangle_{\text{past}}$ looks sharper and shifted to higher values. The ratio between present and average past SFRs is usually called the birthrate parameter $b = \text{SFR}_{\text{current}} / \langle \text{SFR} \rangle_{\text{past}}$. The mean value of this parameter is largely conditioned by the high values of the starbursting interacting systems, so we take the median, 0.68, as a more representative value of the whole sample.

The absolute magnitude of each satellite versus $\log b$ is shown in Figure 8. The region with higher values of the b -parameter is occupied by the four starbursting interacting galaxies and by NGC 3154a. The b -values for these galaxies are in the range 3–9. We notice a weak trend in the sense that brighter satellites

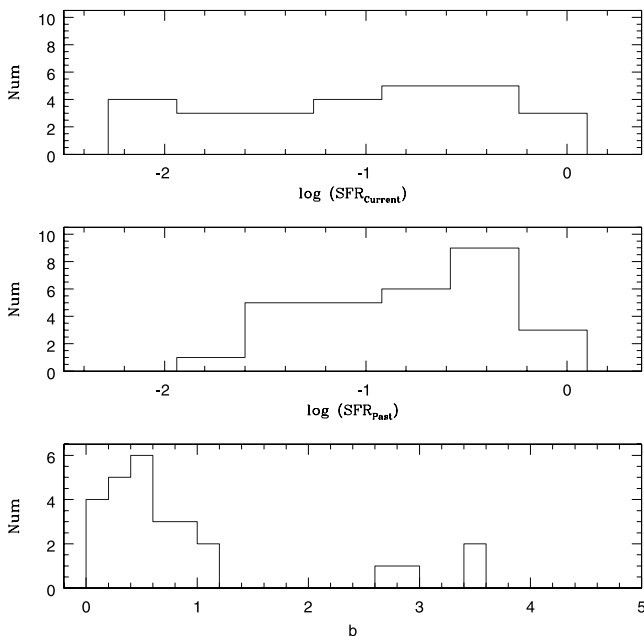


FIG. 7.—Distribution of current (*top*) and past (*middle*) SFRs for the sample of satellite galaxies analyzed in this paper. The bottom panel shows the distribution of the stellar birthrate parameter, $b = \text{SFR}_{\text{current}} / \langle \text{SFR} \rangle_{\text{past}}$.

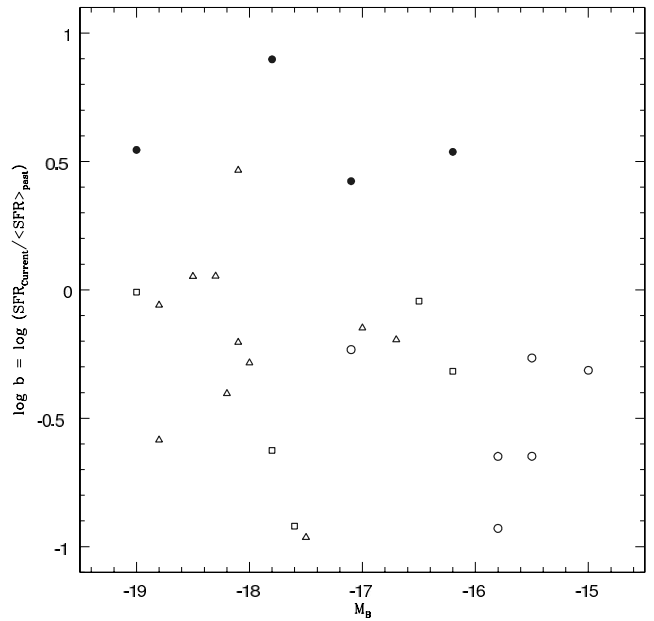


FIG. 8.—Stellar birthrate parameter as a function of the absolute magnitude (M_B), in satellite galaxies for different Hubble morphological types: irregular galaxies (*open circles*), Sb/Sc (*triangles*), and Sa (*squares*). Interacting galaxies are indicated by filled circles.

seem to have a comparatively higher current activity; in fact, four of the five brightest galaxies (excluding the interacting systems) have $b \sim 1$, which seems to indicate that these galaxies are still able to maintain at present their mean past SFR. The global tendency of decline in SFR with cosmological time is expected according to simulations by Mayer et al. (2001). The values of b in any of the morphological types (excluding the interacting systems) range over roughly an order of magnitude, which probably indicates a great variety of star formation histories. The distribution of b (see Fig. 7) is qualitatively similar to that found by van Zee (2001). We do not notice any clear differences between the different morphological types, but given the small sizes of the sample we have not tried to quantify this accurately.

Another way to compare the relevant timescales for the star formation evolution is by computing how much time (t_{form}) the galaxy would have needed to form all the stellar content at the current SFR, and what the maximum time (t_{gas}) would be that the galaxy can continue forming stars at the current rate. The analysis of this in conjunction with optical luminosities and current star formation allow a first approximation to the evolution of the galaxy over cosmic times. An accurate limit for t_{gas} can be estimated simply by dividing the current gas content by the current SFR. This of course would correspond to an ideal case in which all the gas would be converted into stars, and no losses or accretion would occur. Using LEDA,⁵ we have compiled the existing H I measurements as a way to estimate the gas content in each galaxy. These are presented in Table 3, column (4). The values of t_{gas} indicate that the current gas content would be enough to fuel the star formation at the current SFR at least during another Hubble time. For about one-third of the galaxies t_{form} exceeds the Hubble time, so that we conclude again that on average the SFR was higher in the past. As expected, the starbursting galaxies NGC 2718b, NGC 4541e, NGC 5965a₁, and NGC 5965a₂ are among the objects with the lowest formation

⁵ See <http://leda.univ-lyon1.fr>.

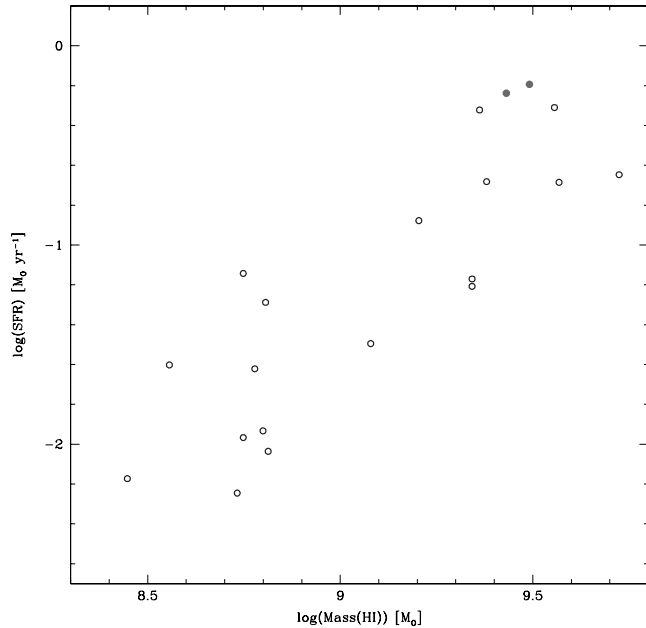


FIG. 9.—Current SFR estimated from $H\alpha$ measurement vs. $H\text{ I}$ mass of the gas. Interacting galaxies, NGC 2718b and NGC 5965a (computed in an aperture enclosing both galaxies, NGC 5965a₁ and 5965a₂), are indicated by filled symbols.

times (also NGC 3154a, which is the satellite galaxy in our sample closest to its parent).

Previous studies (e.g., Casoli et al. 1996) have shown that SFR in spiral galaxies is correlated with the mass of molecular and atomic gas. Our results confirm that relation as illustrated in Figure 9. The correlation extends 1 and 2 orders of magnitude in gas mass and SFR, respectively. NGC 2718b, one of the interacting galaxies, has the largest SFR in the sample and is also one of the galaxies with higher gas content. This seems to reinforce the scenario of significant accretion of gas from NGC 2718a as outlined in § 5.

Figure 10 presents t_{gas} versus t_{form} for our sample of satellite galaxies and compares these timescales with those for four other samples taken from the literature: the Sculptor group dwarf irregular galaxies (dIrrs) studied by Skillman et al. (2003), the Local Group dIrrs of Mateo (1998), the gas-rich low surface brightness galaxies studied by van Zee et al. (1997), and the isolated dIrrs of van Zee (2000, 2001). The figure shows a clear direct correlation between both timescales. The range of magnitudes and the selection effects are different for each sample, so that it is difficult to extract statistical conclusions, although all the samples tend to follow common tendencies.

7. SUMMARY

We have carried out a detailed analysis of narrowband observations of the $H\alpha$ emission in a sample of 31 satellites orbiting giant spiral isolated galaxies. The objects studied span the range $-19 < M_B < -15$ mag and were selected according to relative brightness (at least 2.2 mag fainter than their parents), projected distance (< 500 kpc), and relative velocity (< 500 km s⁻¹) from the primaries. We have presented imaging and photometry in a narrow filter band covering the position of the $H\alpha$ line. The results can be summarized as follows:

1. In all the spiral and irregular satellites (29 objects) we detected $H\alpha$ fluxes above 1.15×10^{-14} ergs s⁻¹ cm⁻². The

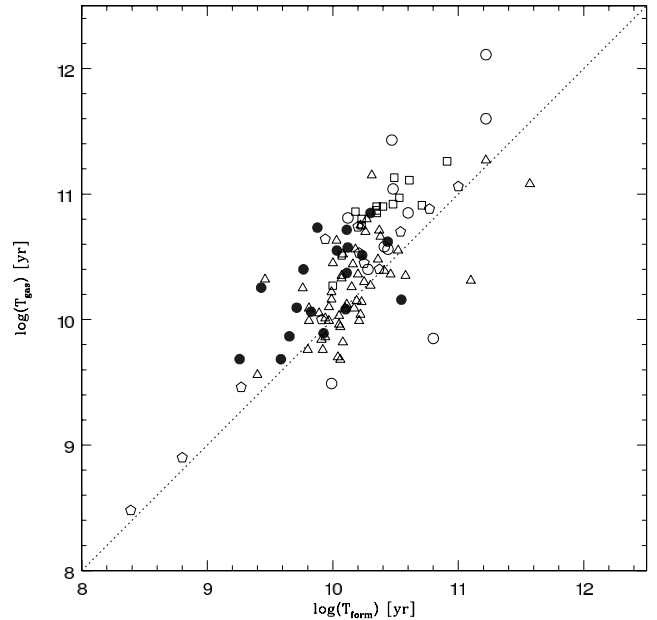


FIG. 10.—Comparison between the ratio of the gas mass to the current SFR (T_{gas}) and the ratio of the luminosity to the current SFR (T_{form}) for the satellite galaxies (filled circles) and for four samples taken from the literature: the Sculptor group dIrrs studied by Skillman et al. (2003; open circles), the Local Group dIrrs of Mateo (1998; pentagons), the gas-rich low surface brightness galaxies studied by van Zee et al. (1997; squares), and the isolated dIrrs of van Zee (2000, 2001; triangles).

inferred current star formation rates are in the range $0.006\text{--}3.66 M_{\odot} \text{ yr}^{-1}$.

2. There are three cases of clear interacting pairs. Four of the galaxies in these pairs are among the objects with higher star-forming activity. In contrast, the only two galaxies of the sample that are not forming stars are also members of these pairs. We do not detect $H\alpha$ emission in the filaments associated with these interactions.

3. The object with the largest current SFR (apart from the interacting systems) corresponds to the satellite galaxy NGC 3154a, which has the smallest projected distance from its progenitor (19 kpc), and the SFR could be due to interaction with the parent galaxy.

4. The median of the birthrate parameter b is 0.68, indicating a fall in activity with cosmic time. Assuming perfect efficiency, the current gas content of the galaxies is enough to fuel this activity for more than another Hubble time.

We thank S. Laine, who read the manuscript and gave us very useful hints and comments. We also thank F. Prada, who participated in the first stages of this project. E. D. Skillman has kindly provided the data used for the comparison presented in Figure 10. S. A. was supported by the Consejo Nacional de Investigaciones Científicas y Técnicas and by a Marie Curie Fellowship of the European Community, program MEST-CT-2004-504604.

APPENDIX

This appendix contains a description of the $H\alpha$ emission maps of each galaxy:

NGC 488c: This is a low surface brightness irregular galaxy in which we notice four main knots with $H\alpha$ emission located in the outer parts of the galaxy.

NGC 772b: What seems to be a bright foreground star is projected through the east side of the galaxy. The $H\alpha$ emission is concentrated in a few discrete spots, the two brightest being situated to the northeast.

NGC 772c: There are diffuse and discrete $H\alpha$ emission features. The two brightest spots are situated roughly symmetrically with respect to the galactic center.

NGC 1517a: There are about 10 $H\alpha$ regions, which are particularly bright in the external parts of the galaxy. Two of the $H\alpha$ features through the west are clearly differentiated from the main body of the disk.

NGC 1620a: The galaxy is irregular, with two to three plumes emerging from the west. In one of these plumes there are a few discrete features with $H\alpha$ emission. The rest of the emission is concentrated in a few features distributed over the full galaxy.

NGC 1961a: A few clumpy small and faint structures are detected in the image after continuum subtraction.

NGC 1961b: This is a luminous spiral satellite galaxy that has a bright pointlike structure close to the center. The $H\alpha$ continuum-subtracted image shows diffuse $H\alpha$ emission with a few superposed features concentrated along two chains in the northeast-southwest direction, enclosing the central part of the galaxy. The brightest spot at $3''$ from the geometric center was suspected to be a foreground star, but it is the dominant component in the continuum-free image, so we think it is a real galactic feature (or an intruder) experiencing a strong starburst.

NGC 1961c: This galaxy is a face-on spiral with a very rich structure in $H\alpha$ emission and several extended features. The two more intense structures are situated in the geometric center and in a spot to the northwest that is also obvious in the R -band image.

NGC 2424b: This is a very irregular galaxy that shows a clumpy structure in the broadband image. The $H\alpha$ continuum-free image shows about six discrete spots, with the most intense one located to the southwest of the galactic center.

NGC 2718a and NGC 2718b: These galaxies are a clear pair of interacting satellites and have a sharp and very straight bridge ($\approx 92''$ [25 kpc]) connecting them. Close to NGC 2718a and perpendicular to the main axis there is what could be a small companion. The continuum-free image shows that the only component with $H\alpha$ emission is NGC 2718b, which has three to four intense knots.

NGC 2775a: The two brightest $H\alpha$ emission features are projected very close and are only partially resolved. The position coincides with the geometric center of the galaxy. Most of the remaining emission is concentrated in a few spots situated to the southeast of the galaxy.

NGC 2775c: This galaxy shows intense $H\alpha$ emission with a very irregular spatial distribution concentrated mainly in the northern part. A differentiated feature is to the southeast of the galaxy. The broadband image shows in that position a plume emerging from the main body of the galaxy.

NGC 2916a: The $H\alpha$ -subtracted image shows an intense and diffuse structure along the major axis. There are two less intense knots situated at the east and west edges of the galaxy.

NGC 3043a: There is an extended diffuse structure in which it is possible to distinguish at least five differentiated regions distributed through the full area (but avoiding the geometric center) of the galaxy.

NGC 3154a: The $H\alpha$ emission is spread over the full projected area of the galaxy in the form of diffuse emission and discrete knots. The most intense spot is located at the geometric center. This is the galaxy in our sample that has the smallest projected distance from its progenitor and (apart from the in-

teracting galaxies) is the one with largest $H\alpha$ luminosity. Although this could be related to a possible interaction with its parent, we do not notice the relevant signs of geometric distortion in the satellite.

NGC 3735a: The $H\alpha$ emission is concentrated in the east side of the galaxy. In particular, there is a bright feature at the geometric center and a few other less intense features in structures resembling arms. In the broadband image there is some evidence of a tail connecting this galaxy and another smaller one of unknown redshift situated to the northeast. However, this last galaxy does not show any $H\alpha$ emission.

NGC 4030b: The majority of the $H\alpha$ emission is concentrated in four discrete spots. One is located at the center, and another is situated to the northwest, coincident with what we have identified as a possible small interacting galaxy. Unfortunately, the redshift of this last object is unknown.

NGC 4541a: The broadband image shows a spiral edge-on galaxy with two small structures perpendicular to the major axis on both edges. The $H\alpha$ continuum-free image shows a diffuse structure that extends over most of the projected area of the galaxy, and some very clumpy structure. This emission seems to be asymmetrically distributed through the southwest, where one of the features mentioned in the broadband image shows clear evidence of $H\alpha$ emission. We think that this could be a small interacting object that could be enhancing the star formation in the neighboring regions of the main galaxy.

NGC 4541b and NGC 4541e: This pair of galaxies is separated by $\sim 41''$. The galaxies have morphological types E and S0/Sa, respectively. In the broadband image there are two tidal tails emerging from NGC 4541b. One of them is pointing directly to NGC 4541e, and it seems clear that its origin is interaction with this galaxy. The other, pointing nearly in the opposite direction, seems more extended and is possibly the relic of a previous passage of this galaxy near NGC 4541e. The continuum-subtracted $H\alpha$ image shows an intense structure in NGC 4541e, while NGC 4541b has no $H\alpha$ emission. The $H\alpha$ emission in NGC 4541e seems to be composed of at least four major clumps located in the main body of the galaxy. A few faint features seem to follow two arms in approximately opposite directions.

NGC 4725a: This is the largest satellite in our sample. The morphology corresponds to a late spiral with clear signs of distortions and possibly dust obscuration. In particular, a plume emerges in the northeast direction. The $H\alpha$ emission is concentrated along the major axis with two bright spots, one approximately in the geometric center and the other to the southwest.

NGC 5248a: The $H\alpha$ features are distributed over the full projected area of the galaxy in about a dozen faint independent features.

NGC 5248b: The brightest spot is located at the geometric center with a number of diffuse structures distributed through the disk.

NGC 5899a: The galaxy shows a rich structure with diffuse $H\alpha$ features extending over the disk and three major discrete features, one in the center and the other two in the northwest direction. A line of diffuse $H\alpha$ emission seems to cross the galaxy in a direction perpendicular to the major axis. We think this is an example of extraplanar diffuse ionized gas.

NGC 5962d: The $H\alpha$ emission features are distributed in numerous discrete features in the disk, avoiding the central part of the galaxy.

NGC 5965a: This really corresponds to two close galaxies, as was noted by Zwicky (1971) and Gutiérrez & Azzaro (2004), separated by $\sim 7''.4$. Following the notation of that paper, we denote them as NGC 5965a₁ and NGC 5965a₂ (other authors

have denoted the two members of this pair as SBS 1533+574b and SBS 1533+574a, respectively). The continuum-subtracted image shows that both components have $H\alpha$ emission. In the northwest component it is possible to recognize at least two irregular features. The isophotes of the northwest component are elongated in the direction of the companion. In addition, the system is surrounded by a diffuse halo.

NGC 6181a: This is a late-type spiral with evident signs of distortion in the broadband image. The $H\alpha$ continuum-free image shows a complex structure dominated by a bright discrete feature that shows at least three bright spots. It seems that this spot corresponds to a structure that is differentiated from the main body of the galaxy and could correspond to a minor merger.

NGC 7137a: The $H\alpha$ emission is concentrated in two extended features situated on the east side of the galaxy. The brightest runs in a direction perpendicular to the main axis.

NGC 7678a: This nice face-on spiral galaxy has $H\alpha$ emission in the form of discrete features in the center and in a ring surrounding the galaxy and approximately tracing the spiral structure. A small galaxy is located very close by to the northwest. This does not show any $H\alpha$ emission. The main $H\alpha$ -emitting regions are located in two extended regions situated in the northeast part of the galaxy. Two plumes of diffuse material seem to connect these two structures with the main body of the galaxy. We think that they could be two separate structures in the process of strong interaction with the main galaxy.

REFERENCES

- Alonso, M. S., Tissera, P. B., Coldwell, G., & Lambas, D. G. 2004, *MNRAS*, 352, 1081
- Barton, E. J., Geller, M. J., & Kenyon, S. J. 2000, *ApJ*, 530, 660
- Bell, E. F. 2003, *ApJ*, 586, 794
- Bergvall, N., Laurikainen, E., & Aalto, S. 2003, *A&A*, 405, 31
- Bertin, E., & Arnouts, S. 1996, *A&AS*, 117, 393
- Brinchmann, J., Charlot, S., White, S. D. M., Tremonti, C., Kauffmann, G., Heckman, T., & Brinkmann, J. 2004, *MNRAS*, 351, 1151
- Casoli, F., Dickey, J., Kazes, I., Boselli, A., Gavazzi, P., & Baumgardt, K. 1996, *A&A*, 309, 43
- Colless, M., et al. 2001, *MNRAS*, 328, 1039
- Dijkstra, M., Haiman, Z., Rees, M. J., & Weinberg, D. H. 2004, *ApJ*, 601, 666
- Donzelli, C. J., & Pastoriza, M. G. 1997, *ApJS*, 111, 181
- Gil de Paz, A., Madore, B. F., & Pevunova, O. 2003, *ApJS*, 147, 29
- Gutiérrez, C. M., & Azzaro, M. 2004, *ApJS*, 155, 395
- Gutiérrez, C. M., Azzaro, M., & Prada, F. 2002, *ApJS*, 141, 61
- Hopkins, A. M., Schulte-Ladbeck, R. E., & Drozdovsky, I. O. 2002, *AJ*, 124, 862
- Kauffmann, G., White, S. D. M., & Guiderdoni, B. 1993, *MNRAS*, 264, 201
- Kennicutt, R. C., Jr. 1992, *ApJS*, 79, 255
- . 1998, *ARA&A*, 36, 189
- Klypin, A., Kravtsov, A. V., Valenzuela, O., & Prada, F. 1999, *ApJ*, 522, 82
- Knebe, A., Gill, S. P. D., & Gibson, B. K. 2004, *Publ. Astron. Soc. Australia*, 21, 216
- Knebe, A., Power, C., Gill, S. P. D., & Gibson, B. K. 2006, *MNRAS*, 368, 741
- Kong, X. 2004, *A&A*, 425, 417
- Kong, X., Cheng, F. Z., Weiss, A., & Charlot, S. 2002, *A&A*, 396, 503
- Kron, R. G. 1980, *ApJS*, 43, 305
- Lambas, D. G., Tissera, P. B., Alonso, M. S., & Coldwell, G. 2003, *MNRAS*, 346, 1189
- Mateo, M. L. 1998, *ARA&A*, 36, 435
- Mayer, L., Governato, F., Colpi, M., Moore, B., Quinn, T., Wadsley, J., Stadel, J., & Lake, G. 2001, *ApJ*, 559, 754
- Mendez, D. I., Esteban, C., & Balcells, M. 1999, *AJ*, 117, 1229
- Moore, B., Ghigna, S., Governato, F., Lake, G., Quinn, T., Stadel, J., & Tozzi, P. 1999, *ApJ*, 524, L19
- Oke, J. B. 1990, *AJ*, 99, 1621
- Salpeter, E. E. 1955, *ApJ*, 121, 161
- Sekiguchi, K., & Wolstencroft, R. D. 1992, *MNRAS*, 255, 581
- Skillman, E. D., Cote, S., & Miller, B. W. 2003, *AJ*, 125, 593
- Somerville, R. 2002, *ApJ*, 572, L23
- van Zee, L. 2000, *AJ*, 119, 2757
- . 2001, *AJ*, 121, 2003
- van Zee, L., Haynes, M. P., & Salzer, J. J. 1997, *AJ*, 114, 2479
- White, S. D. M., & Rees, M. J. 1978, *MNRAS*, 183, 341
- Willman, B., Governato, F., Dalcanton, J. J., Reed, D., & Quinn, T. 2004, *MNRAS*, 353, 639
- Zaritsky, D., Smith, R., Frenk, C., & White, S. D. M. 1997, *ApJ*, 478, 39
- Zwicky, F. 1971, *Catalogue of Selected Compact Galaxies and of Post-Eruptive Galaxies* (Guemligen: Zwicky)